frontiers in Environmental Science

ORIGINAL RESEARCH
published: 04 March 2022
doi: 10.3389/fenvs.2022.842237

Spatiotemporal Distributions of $PM_{2.5}$ Concentrations in the Beijing–Tianjin–Hebei Region From 2013 to 2020

Xiaohui Yang[1,2,3], *Dengpan Xiao*[1,2,3]*, *Huizi Bai*[3], *Jianzhao Tang*[3] *and Wei Wang*[1,2]*

[1]College of Geography Science, Hebei Normal University, Shijiazhuang, China, [2]Hebei Laboratory of Environmental Evolution and Ecological Construction, Shijiazhuang, China, [3]Institute of Geographical Sciences, Hebei Academy of Sciences, Hebei Engineering Research Center for Geographic Information Application, Shijiazhuang, China

Fine particulate matter ($PM_{2.5}$) seriously affects the environment, climate, and human health. Over the past decades, the Beijing–Tianjin–Hebei region (BTH) has been severely affected by pollutant gas and $PM_{2.5}$ emissions caused by heavy industrial production, topography, and other factors and has been one of the most polluted areas in China. Currently, the long-term, large-scale, and high spatial resolution monitoring $PM_{2.5}$ concentrations ([$PM_{2.5}$]) using satellite remote sensing technology is an important task for the prevention and control of air pollution. The aerosol optical depth (AOD) retrieved by satellites combined with a variety of auxiliary information was widely used to estimate [$PM_{2.5}$]. In this study, a two-stage statistical regression [linear mixed effects (LME) + geographically weighted regression (GWR)] model, combined with the latest high spatial resolution (1 km) AOD product and meteorological and land use parameters, was constructed to estimate [$PM_{2.5}$] in BTH from 2013 to 2020. The model was fitted annually, and the ranges of coefficient of determination (R^2), root mean square prediction errors (*RMSPE*), and relative prediction error (*RPE*) for the model cross-validation were 0.85–0.95, 7.87–29.90 μg/m^3, and 19.19%–32.71%, respectively. Overall, the model obtained relatively good performance and could effectively estimate [$PM_{2.5}$] in BTH. The [$PM_{2.5}$] showed obvious temporal characteristic within a year (high in winter and low in summer) and spatial characteristic (high in the southern plain and low in the northern mountain). During the investigated period of 2013–2020, the high pollutant areas ([$PM_{2.5}$] > 75 μg/m^3) in 2020 significantly narrowed compared to 2013, and the annual average [$PM_{2.5}$] in BTH fell below 55 μg/m^3, with a drop of 54.04%. In particular, the [$PM_{2.5}$] in winter season dropped sharply from 2015 to 2017 and declined steadily after 2017. Our results suggested that significant achievements have been made in air pollution control over the past 8 years, and they still need to be maintained. The research can provide scientific basis and support for the prevention and control of air pollution in BTH and beyond.

Keywords: $PM_{2.5}$ concentrations, aerosol optical depth, two-stage statistical regression model, spatiotemporal distribution, Beijing–Tianjin–Hebei region, Tianjin–Hebei region

OPEN ACCESS

Edited by:
Jianhuai Ye,
Southern University of Science and Technology, China

Reviewed by:
Jie Zhang,
University at Albany, United States
Xiaodong Xie,
Nanjing University of Information Science and Technology, China

***Correspondence:**
Dengpan Xiao
xiaodp@sjziam.ac.cn
Wei Wang
wangwei@hebtu.edu.cn

Specialty section:
This article was submitted to Atmosphere and Climate, a section of the journal Frontiers in Environmental Science

Received: *23 December 2021*
Accepted: *19 January 2022*
Published: *04 March 2022*

Citation:
Yang X, Xiao D, Bai H, Tang J and Wang W (2022) Spatiotemporal Distributions of $PM_{2.5}$ Concentrations in the Beijing–Tianjin–Hebei Region From 2013 to 2020. Front. Environ. Sci. 10:842237. doi: 10.3389/fenvs.2022.842237

INTRODUCTION

Fine particulate matter ($PM_{2.5}$, particles with aerodynamic diameter less than 2.5 μm) are suspended in the atmosphere as a composite of solid and liquid particles. It can carry toxic and harmful substances over long distances, crossing countries and geographic boundaries (Engel-Cox et al., 2013; Li et al., 2017). Epidemiological studies have shown that exposure to high $PM_{2.5}$ concentrations ([$PM_{2.5}$]) has adverse effects on human health, such as increasing morbidity and mortality of cardiopulmonary diseases (Chow et al., 2006; Gu et al., 2018; Riediker et al., 2018; Zhang et al., 2018). With the rapid economic and urbanization development, $PM_{2.5}$ has become a major air pollutant in China, especially in densely populated urban agglomerations, such as the Beijing–Tianjin–Hebei region (BTH) and the Yangtze River Delta region (He and Huang, 2018a; Wang G. et al., 2021). Therefore, studying the spatiotemporal patterns and trends of [$PM_{2.5}$] is conductive to taking accurate preventive measures against $PM_{2.5}$ pollution for policymakers and has important practical significance for air pollution control (Yan et al., 2021).

At present, $PM_{2.5}$ monitoring data mainly were derived from the ground monitoring network and aerosol optical depth (AOD) products generated by satellite sensors (van Donkelaar et al., 2006; Chudnovsky et al., 2014). AOD is a measure of the degree about which aerosols prevent light from penetrating the atmosphere and describes the reduction effect of aerosols on light. The AOD retrieved by visible channels is most sensitive to particles with sizes between 0.1 and 2 μm (close to the particle size of $PM_{2.5}$), which is an important theoretical basis for establishing the correlation between AOD and $PM_{2.5}$ (Kahn er al., 1998; Hu et al., 2013). Generally, satellite-derived AOD can provide valuable information for the estimation of ground-level $PM_{2.5}$ pollution due to its large spatial coverage, high spatial resolution, and reliable repeated measurement, especially suitable for those places without $PM_{2.5}$ monitoring station on the surface (Schaap et al., 2009; Yeganeh et al., 2017; Stowell et al., 2020). Recently, most of the AOD products used to predict [$PM_{2.5}$] were derived from the Moderate Resolution Imaging Spectroradiometer (MODIS), Visible Infrared Imaging Radiometer Suite (VIIRS), Multiangle Imaging SpectroRadiometer (MISR), and Advanced Himawari Imager (AHI) that the nominal spatial resolutions for AOD retrieved by their algorithms are 10 or 3 km, 17.6 or 4.4, 0.75 and 5 km, respectively (Lee et al., 2011; Hu et al., 2014a; Yao et al., 2018; Wang et al., 2020). However, the coarser resolution AOD products hinder the study of fine-scale [$PM_{2.5}$]. For example, the detailed spatial variability of $PM_{2.5}$ exposure was ignored at the urban scale (Hu et al., 2014b). A new high spatial resolution (1-km) MODIS Collection 6 (C6) daily AOD product (MCD19A2) was released in 2018, which was generated based on the Multi-Angle Implementation of Atmospheric Correction (MAIAC) algorithm and demonstrated excellent performance in estimating [$PM_{2.5}$] (Lyapustin et al., 2018; Zhang Z. et al., 2019; Choi et al., 2019).

Previous studies have established a variety of models to explore the relationship between station-based $PM_{2.5}$ observations and satellite-based AOD data, including scaling approach (Liu et al., 2004), semi-empirical (Wang and Christopher, 2003), and statistical regression models. Given their simplicity, fast process, and high performance, statistical regression models are widely used. These models ranged from simple linear regression (Engel-cox et al., 2004) in early study to advanced statistical models, such as linear mixed effects (LME) (Lee et al., 2011), generalized additive (GAM) (Liu et al., 2009), geographically weighted regression (GWR) (Hu et al., 2013), space-time LME (STLME) (Wang W. et al., 2021), geographically and temporally weighted regression (GTWR) (Bai et al., 2016), and time fixed effects regression (TEFR) (Yao et al., 2018). To improve prediction accuracy, various models have evolved from using AOD as the only predictor to a combination of multiple additional predictors [e.g., meteorological factors, human activities, and land use (LU) variables] (Gupta and Christopher, 2009; Hu et al., 2017). To reduce the deviation caused by a single model prediction, more complex models were then developed by combining two or more models, such as two-stage model (e.g., LME + GWR, LME + GAM, and TEFR + GWR) (Ma et al., 2016; Yao et al., 2019; Xue et al., 2020; Guo et al., 2021) and three-stage model [e.g., inverse probability weighting (IPW) + generalized additive mixed model (GAMM) + kriging with external drift (KED)] (Liang et al., 2018). In addition, some machine learning methods were employed to estimate [$PM_{2.5}$], such as random forest (RF) (Stafoggia et al., 2019; Zhao et al., 2020), artificial neural network (ANN) (Polezer et al., 2018), adaptive deep neural network (SADNN) (Chen et al., 2021), and support vector machine (SVM) (Moazami et al., 2016). However, the parameters in the machine learning models cannot explain the spatiotemporal relationship between $PM_{2.5}$ and AOD, owing to an unknown mechanism, causing the model to lack reasoning capability (Yang et al., 2021). The LME + GWR model is weak in dealing with nonlinear relationships between various predictors, but it can accurately capture the spatiotemporal variability of $PM_{2.5}$–AOD, which is better than the LME model and LME + GAM model (Zhang K. et al., 2019; Guo et al., 2021). Moreover, related studies indicated that adding interaction terms (quadratic terms) to the statistical regression models could better describe nonlinear effects (Xiao et al., 2017; He et al., 2020).

$PM_{2.5}$ estimation data with higher resolution and long-term series are of great significance for the analysis of small-scale air pollution (Lu et al., 2021). In this study, our main goal was to estimate the [$PM_{2.5}$] in the BTH and analyze its long-term spatiotemporal characteristics and trends. The specific objectives of this research were 1) to establish a suitable two-stage statistical regression model (LME + GWR), including adding quadratic terms and interaction terms in the model to account for the nonlinear relationship, and considering the influence of meteorological and LU information and AOD data in the BTH; 2) to estimate the daily [$PM_{2.5}$] distribution with 1-km spatial resolution in the BTH from 2013 to 2020; and 3) to analyze the spatiotemporal characteristics and trends of long-term [$PM_{2.5}$] on annual, seasonal, and monthly scales. The results can provide a reference for the joint prevention and control of particulate pollution in the study area.

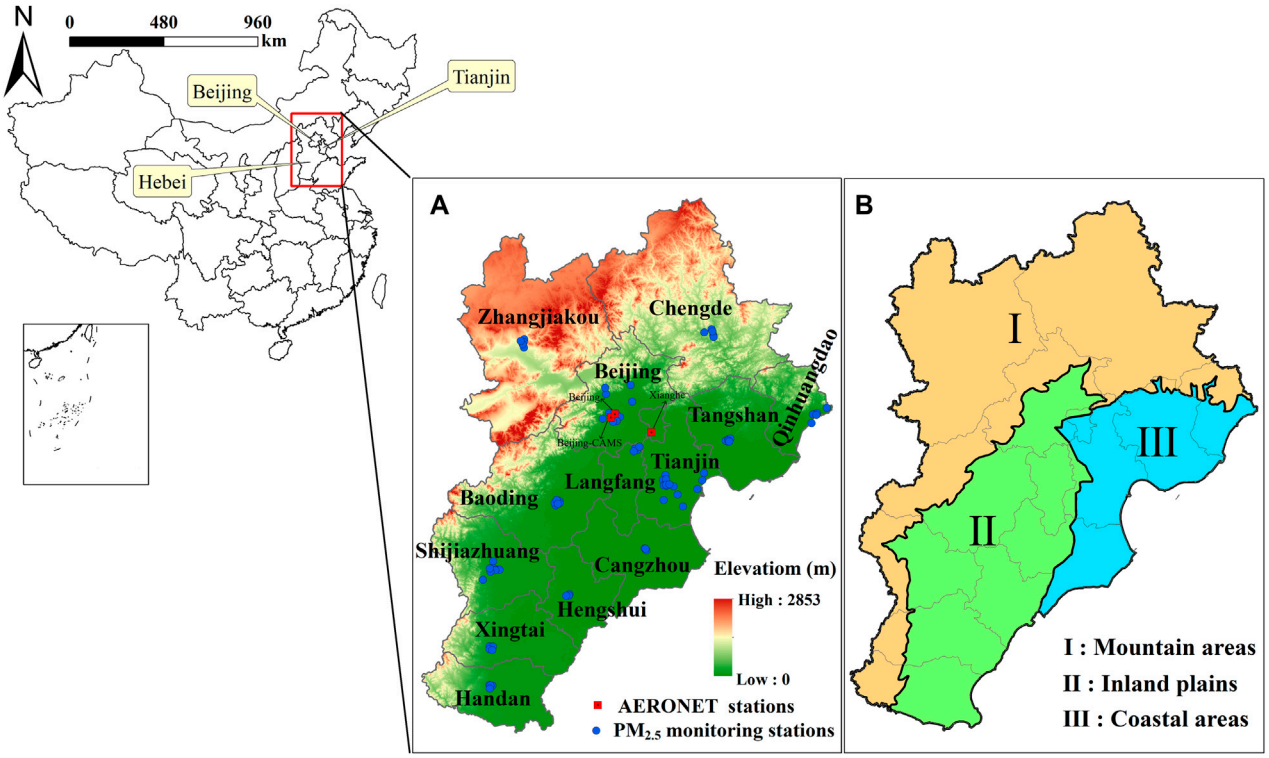

FIGURE 1 | Study area with 80 monitoring stations in the Beijing–Tianjin–Hebei region **(A)** and sub-areas **(B)** divided by terrain.

MATERIALS

Study Area

The BTH (113.45°E–119.85°E and 36.03°N–42.62°N) is one of the most important administrative, commercial, and cultural center in northern China, including Beijing and Tianjin, and 11 prefecture-level cities of Hebei Province (**Figure 1**). The region is densely populated and is a secondary industry that used coal as the main energy source emits various air pollutants, which causing relatively severe haze (Zhao et al., 2019). In particular, in the inland plains, coupled with unfavorable topography, it makes it more difficult for pollutants to spread (Lv et al., 2017). According to the statistics from the "China Environmental Bulletin" (http://www.cnemc.cn/jcbg/zghjzkgb/) during 2013–2020, the BTH included seven, eight, seven, six, six, five, four, and one, respectively, among the top 10 cities with poor air quality in China. Although the air quality in this region has improved during the past few years, we should still pay close attention to $PM_{2.5}$ pollution. Therefore, it is essential to analyze the spatiotemporal distribution and the trend of [$PM_{2.5}$].

$PM_{2.5}$ Monitoring Data and Predictor Variables

In addition to adding AOD to the model for [$PM_{2.5}$] prediction, it has been recognized that combining meteorological and LU information can significantly improve the model predictability (Hu et al., 2017; Wang G. et al., 2021). In this study, for the proposed two-stage statistical regression (LME + GWR) model, a main independent predictor (AOD) and eight auxiliary predictors [i.e., planetary boundary layer height (PBLH), 2-m air temperature (TEMP), 10-m wind speed (WS), relative humidity (RH, specific humidity calculated), surface pressure (PRS), precipitation (PRCP), forest coverage (FC), and urban coverage (UC)] were utilized through variables selection and multicollinearity diagnosis. The datasets covered the period from January 1, 2013, to December 31, 2020. The detail information about the datasets is shown in **Table 1**.

1) $PM_{2.5}$ data. The $PM_{2.5}$ hourly concentration of 80 monitoring stations in BTH was obtained from the National Urban Air Quality Real-time Release Platform. In the process of fitting the daily mean [$PM_{2.5}$], we eliminated the [$PM_{2.5}$] (i.e., <2 and >500 μg/m^3) that was not within the monitoring range of the National Ambient Air Quality Standard (NAAQS) (GB 3095-2012) to ensure the validity of the $PM_{2.5}$ data.
2) AErosol RObotic NETwork (AERONET) AOD. The AOD measured by AERONET was used as the true value to verify the accuracy of the AOD retrieved by remote sensing. The AERONET AOD data (version 3, level 2) from three sites (i.e., Beijing, Beijing-CAMS, and Xianghe) were collected in our modeling area (https://aeronet.gsfc.nasa.gov/), which were used to validate the MODIS MAIAC AOD.
3) One-kilometer AOD data. High-resolution AOD products are increasingly used to capture the fine-scale differences in the spatial distribution of [$PM_{2.5}$]. The emergence of the MAIAC algorithm provided a theoretical basis for constructing a high-resolution [$PM_{2.5}$] estimation model. The MAIAC Terra/

TABLE 1 | Information about data source, temporal and spatial resolution.

Variable		Temporal resolution	Spatial resolution	Data source
$PM_{2.5}$		hourly	site	http://106.37.208.233:20035/
AOD		daily	1 × 1 km	https://ladsweb.modaps.eosdis.nasa.gov/
Meteorological	PBLH	hourly	0.25° × 0.3125°	ftp://rain.ucis.dal.ca/ctm/
	TEMP, WS, RH, PRS, and PRCP	daily	0.1° × 0.1°	http://data.tpdc.ac.cn/zh-hans/data/ (2013–2018)
			0.0625° × 0.0625°	http://data.cma.cn/ (2019–2020)
Land use	FC	yearly	30 × 30 m	http://www.dsac.cn/DataProduct/
	UC			

PBLH is planetary boundary layer height; TEMP, WS, RH, PRS, and PRCP are 2-m air temperature, 10-m wind speed, relative humidity, surface pressure, and precipitation, respectively. FC and UC are forest coverage and urban coverage, respectively.

Aqua AOD (0.55 μm) products were available through the MODIS Collection-6 data record. The AERONET $AOD_{550\ nm}$ was calculated from the AOD at 675 and 440 nm using the Angstrom exponent. Simple linear regressions were carried out between the MAIAC Terra/Aqua AOD (0.55 μm) and AERONET $AOD_{550\ nm}$ at the AERONET sites for each year. The results show that the fitting with the coefficient of determination (R^2) in 0.81–0.91 was acceptable in all years (**Figure 2**). The root mean square prediction error (*RMSPE*) ranged from 0.10 to 0.25, 73.15%–83.74% of the samples falling within the interval of 1 × variance, and the slope of 0.95–1.17, which met the verification accuracy requirements.

4) Meteorological data. The hourly PBLH data were derived from the Goddard Earth Observing System Model 5-Forward-processing (GEOS5-FP). Other daily meteorological data (e.g., TEMP, WS, RH, PRS, and PRCP) were extracted from the National Tibetan Plateau Data Center (TPDC) and only cover the period from 2013 to 2018 (Yang and He, 2019). The daily data from 2019 to 2020 were downloaded from the National Meteorological Science Data Center. The meteorological data in the two periods have negligible influence on the model prediction results because they have similar spatial resolutions and need to be interpolated to the same resolution as MODIS MAIAC AOD.
5) LU data. LU data were downloaded from the Geographical Information Monitoring Cloud Platform (GIM Cloud). The study selected LU data in 2015 to represent the LU status from 2013 to 2020 and extracted the urban coverage and FC in the study area into the model.
6) Data integration. Considering to match the daily [$PM_{2.5}$], the daily PBLH data were represented by averaging the observation values obtained at two times during the transit of the MODIS satellite. The daily meteorological data were then resampled to the 1-km grid by the bilinear interpolation method. In addition, the UC and FC data with 30-m spatial resolutions were averaged over the 1-km grid.

METHODS

Collinearity Diagnosis

Considering the stability of the predictive model, the collinearity of the independent variables should be diagnosed. In this study, the variance inflation factor (VIF) and tolerance value (TV) were selected to diagnose the collinearity of the selected variables. The VIF and TV of all independent variables participating in the model satisfied VIF < 10 and TV > 0.1 for each year (**Table 2**), indicating that there was no collinearity problem among the independent variables and could be considered for model fitting.

Two-Stage Statistics Regression Model

A two-stage statistical regression model consisting of LME model and GWR model was used to simulate the spatiotemporal variation of the $PM_{2.5}$–AOD relationship. The LME model in the first stage was applied to correct the time-varying relationship of $PM_{2.5}$–AOD. The quadratic term of AOD (AOD^2) and the interaction between PBLH and AOD (PBLH × AOD) were added to the model to explain the nonlinear relationship between AOD and $PM_{2.5}$. The specific structure of the model is as follows:

$$\begin{aligned} PM_{2.5st} = {} & (\beta_0 + \theta_0) + (\beta_1 + \theta_1)AOD_{st} + (\beta_2 + \theta_2)AOD_{st}^2 \\ & + (\beta_3 + \theta_3)PBLH_{st} + (\beta_4 + \theta_4)WS_{st} \\ & + (\beta_5 + \theta_5)TEMP_{st} + (\beta_6 + \theta_6)RH_{st} + (\beta_7 + \theta_7)PRS_{st} \\ & + (\beta_8 + \theta_8)PRCP_{st} + \beta_9 \times PBLH_{st} \times AOD_{st} \\ & + \beta_{10} \times FC_s + \beta_{11} \times UC_s \\ & + \varepsilon_{st}\,(\theta_{1\sim8}) \sim N\left[(0,0,0,\psi)\right], \varepsilon_{st} \sim N(0,\sigma^2) \end{aligned} \quad (1)$$

where $PM_{2.5st}$ is the [$PM_{2.5}$] at station *s* on day *t*; AOD_{st} is the AOD of the grid cell in which the station *s* is positioned on day *t*; AOD^2st is the quadratic term for AOD at station *s* on day *t*; PBLH*st*, WS*st*, TEMP*st*, RH*st*, PRS*st*, and PRCP*st* are the planetary boundary layer height, wind speed at 10-m height, temperature at 2-m height, relative humidity, surface pressure, and precipitation at station *s* on day *t*, respectively; $PBLH_{st} \times AOD_{st}$ is the interaction between PBLH and AOD at station *s* on day *t*; FC_s and UC_s are the FC value and UC value at station *s*, respectively; β_0 and θ_0 are the fixed and random intercepts, respectively; β_1 and β_2 are the fixed slopes of square polynomials for AOD; β_3, β_4, β_5, β_6, β_7, β_8, β_{10}, and β_{11} are the fixed slopes of PBLH, WS, TEMP, RH, PRS, PRCP, FC, and UC; β_9 is the fixed slope of the interaction between PBLH and AOD; θ_1 and θ_2 are the daily random slopes of square polynomials for AOD; and θ_3–θ_8 are the daily random slopes of each meteorological variables, respectively.

The GWR model of the second stage was used to correct the spatial heterogeneity between $PM_{2.5}$ and AOD. The specific method was to model the residuals of the LME model. This GWR model was fitted once a day to account for temporal variability. In addition, the model using adaptive bandwidth selection methods calculated by

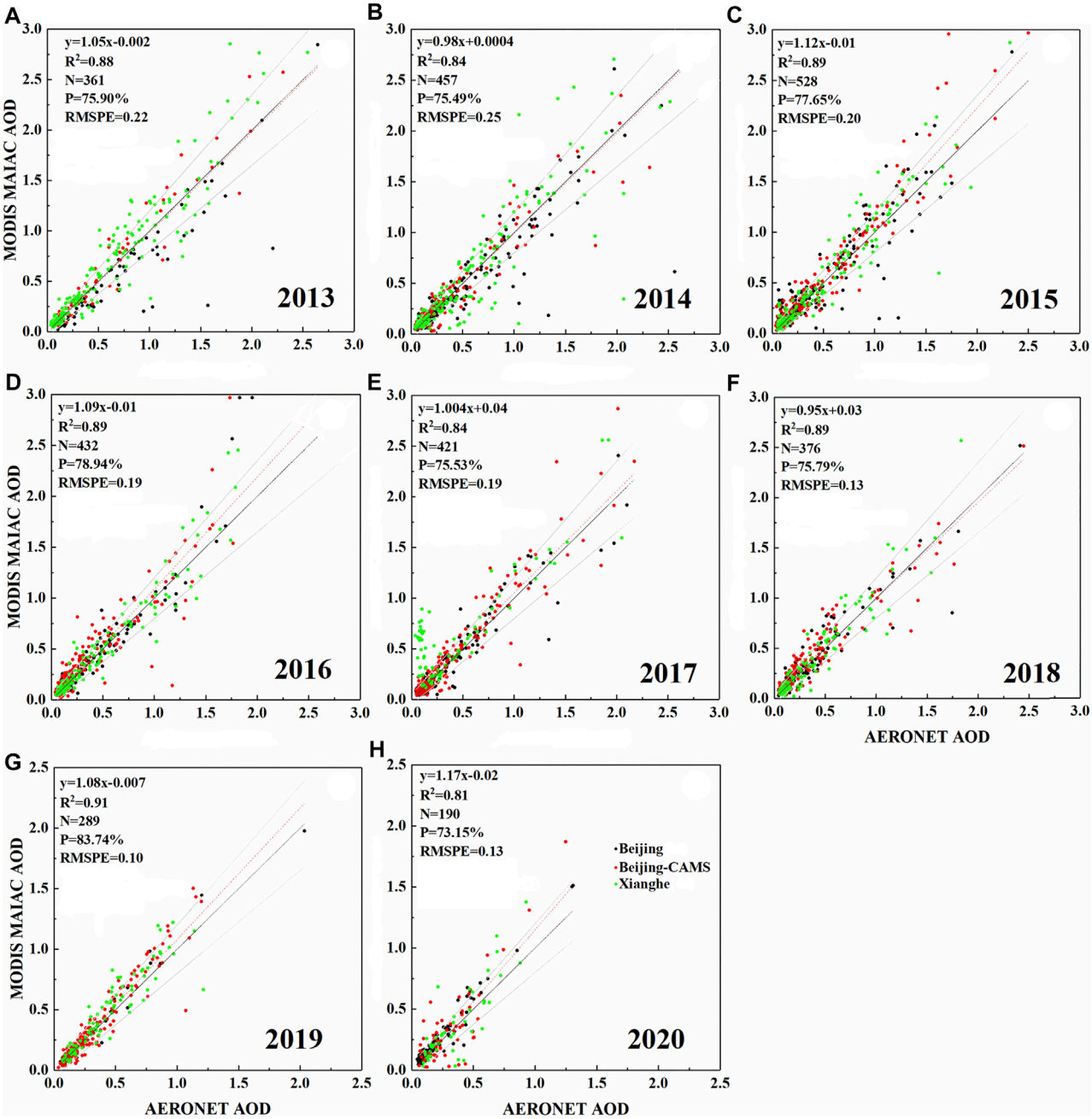

FIGURE 2 | Scatter plot of MODIS MAIAC AOD and AERONET AOD at 550 nm for the period of 2013–2020 **(A–H)**. The red dashed line is the regression line. The black line is a 1:1 line. The gray lines represent the expected error (EE) envelopes [±(0.05 + 20% × AERONET AOD)]. It also shows the coefficient of determination (R^2), the number of samples (N), the percentage in EE (P), and the root mean square prediction error (*RMSPE*).

minimizing the corrected Akaike Information Criterion (AIC) value. The specific expression is as follows:

$$PM_{2.5\_resi_{st}} = \beta_0(u_s, v_s) + \beta_1(u_s, v_s)AOD_{st} + \varepsilon_{st}\ \varepsilon_{st} \sim N(0, \sigma^2) \quad (2)$$

where $PM_{2.5}$_$resi_{st}$ is the residual value from the LME model at station s in day t; AOD_{st} is the AOD value at station s on day t; (u_s, v_s) is the spatial coordinates of the monitoring station s; and β_0 (u_s,v_s) and β_1 (u_s,v_s) represent the regression intercept and regression slope at station s, respectively.

For model verification, a 10-fold cross-validation (CV) method was conducted to detect the degree of overfitting of the model. The entire model-fitting dataset was randomly split into 10 subsets, with each subset containing approximately 10% of the dataset. In each CV time, we selected one subset as the testing sample and used the

TABLE 2 | The range of variance inflation factor (VIF) and tolerance value (TV) in the analysis of variable collinearity.

Predict variables	VIF	TV
AOD	1.18–1.64	0.60–0.84
PBLH	1.17–1.60	0.69–0.84
WS	1.15–1.28	0.68–0.86
TEMP	1.15–1.78	0.56–0.86
RH	1.41–1.88	0.52–0.82
PRS	1.24–1.50	0.66–0.80
PRCP	1.03–1.07	0.93–0.96
FC	1.30–1.48	0.67–0.76
UC	1.43–1.87	0.53–0.69

PBLH is planetary boundary layer height; TEMP, WS, RH, PRS, and PRCP are 2-m air temperature, 10-m wind speed, relative humidity, surface pressure, and precipitation, respectively. FC and UC are forest coverage and urban coverage, respectively.

remaining nine subsets to fit the model for prediction on the testing sample. This process was repeated 10 times to ensure that all the subsets were predicted. We fitted a linear regression was performed between the measured and predicted [$PM_{2.5}$], and the fitted R^2, slope, *RMSPE*, and relative prediction error (*RPE*) were evaluated the performance of the model. They represented by **Eqs. 3** and **4**, respectively.

$$RMSPE = \sqrt{\frac{\sum_{i=1}^{n}\left(y_{mod,i} - y_{obs,i}\right)^2}{n}} \quad (3)$$

$$RPE = \frac{RMSPE \times 100\%}{\bar{y}} \quad (4)$$

where $y_{mod,i}$ is the estimated $PM_{2.5}$ at site *i*; $y_{obs,i}$ is the observed $PM_{2.5}$ at site *i*; *n* is the total number of data samples; and $\bar{y}$ is the average of the observed $PM_{2.5}$.

The estimation process of the daily [$PM_{2.5}$] by the LME + GWR model is shown in **Supplementary Figure S1**.

RESULTS

Descriptive Statistics

As shown in **Table 3**, the daily minimum and maximum [$PM_{2.5}$] in the BTH were ranged from 2 to 3 μg/m^3 and from 371 to 499 μg/m^3, respectively, which indicated that the pollution degree of different areas in the BTH had considerable differences. The annual average [$PM_{2.5}$] during the investigated period from 2013 to 2020 in the BTH were 91.27, 85.93, 72.89, 68.22, 61.02, 53.53, 45.75, and 40.97 μg/m^3, respectively, indicating that the $PM_{2.5}$ pollution has been on a downward trend in the past 8 years. However, it still exceeded the limit (35 μg/m^3) of the national secondary standard for ambient air quality (GB3095-2012). The average annual AOD ranged from 0.37 to 0.69 during the same period. The great difference between the mean FC and UC reflected that most of the monitoring sites in the study area were located inside or around the city. In addition, the ranges of the meteorological variables from 2013 to 2020 are also shown in **Table 3**.

During the period from 2013 to 2020, the monthly [$PM_{2.5}$] monitored in the BTH demonstrated that the median monthly [$PM_{2.5}$] presented a U-shaped oscillation for each year (**Figure 3**). Overall, the [$PM_{2.5}$] displayed significant monthly differences, following the change pattern of "high in winter, low in summer, falling in spring and rising in autumn". In detail, [$PM_{2.5}$] displayed a downward trend from January to May, a general stability from June to September, and an upward trend from October to December. The reason for the highest monthly [$PM_{2.5}$] in December and January was the combined effect of coal-fired heating in winter and unfavorable meteorological conditions in the BTH, such as low air humidity and weak wind speed.

Model-Fitting and Validation

The comparison of LME + GWR model fitting (**Figure 4A**) and 10-fold CV results (**Figure 4B**) from 2013 to 2020 indicated that the model displayed excellent performance in capturing daily [$PM_{2.5}$]. For model fitting, the data distribution was concentrated toward the regression line. The R^2 ranged from 0.89 to 0.97, indicating that the two-stage model could effectively explain 89%–97% of the ground-level [$PM_{2.5}$] variation. The slope ranged from 0.89 to 1.04, indicating that only a small prediction bias remained in the model. In addition, the fitting results also displayed that the *RMSPE* and *RPE* were 6.85–24.60 μg/m^3 and 16.67%–26.94%, respectively. Compared with model fitting, the 10-fold CV results showed that the *CV-R*^{2}, *CV-RMSPE*, and *CV-RPE* ranged from 0.85 to 0.95, 7.87 μg/m^3 to

TABLE 3 | Statistical indicators of modeling variables.

Variables	Minimum	Maximum	Mean	Std. Deviation
$PM_{2.5}$ (μg/m^3)	2.00–3.00	371.00–499.00	40.97–91.27	34.18–77.23
AOD (unitless)	0.003–0.02	2.98–3.79	0.37–0.69	0.37–0.71
PBLH (m)	54.68–64.69	2,307.02–3,124.23	333.92–553.57	321.9–471.71
WS (m/s)	0.05–0.63	5.61–12.04	1.52–2.59	0.73–1.28
TEMP (°C)	–22.66–-12.85	31.58–33.97	9.83–12.88	10.30–11.57
RH	0.04–0.10	0.93–1.00	0.42–0.51	0.16–0.18
PRS (hPa)	866.01–891.61	1,016.94–1,042.73	997.25–1,006.12	27.10–33.92
PRCP (mm)	0	42.02–99.12	0.30–0.43	2.27–2.74
FC	0	0.68–0.75	0.03–0.05	0.11–0.14
UC	0	0.79–1.00	0.55–0.78	0.29–0.33

PBLH is planetary boundary layer height; TEMP, WS, RH, PRS, and PRCP are 2-m air temperature, 10-m wind speed, relative humidity, surface pressure, and precipitation, respectively. FC and UC are forest coverage and urban coverage, respectively.

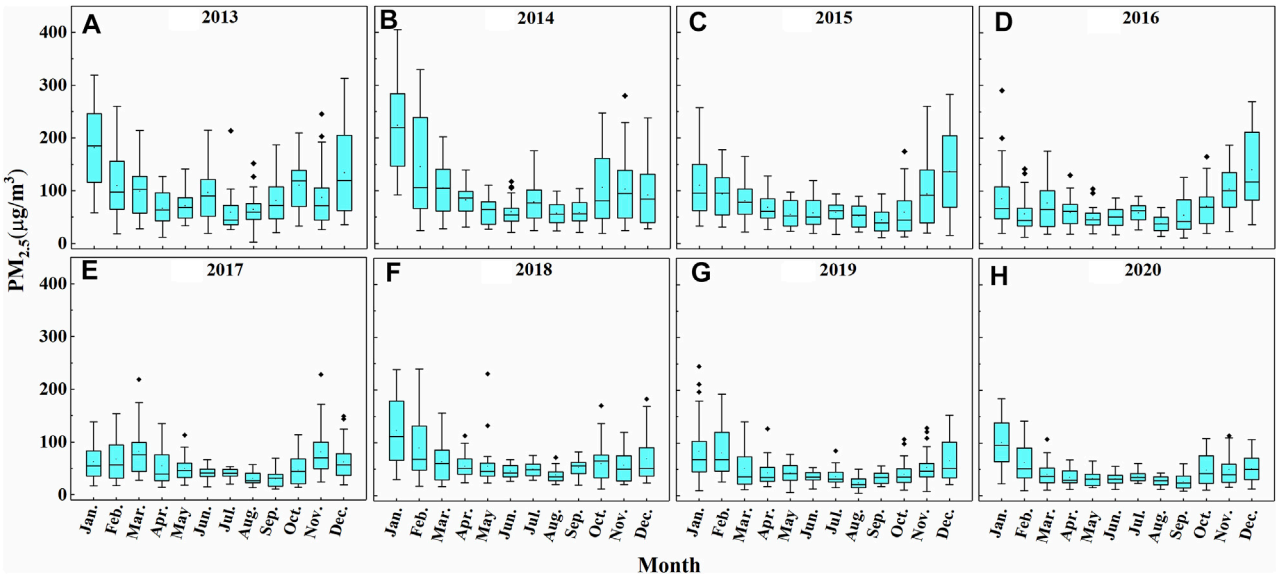

FIGURE 3 | The monthly mean observed $PM_{2.5}$ concentrations from 2013 to 2020 **(A–H)** in the Beijing–Tianjin–Hebei region.

29.90 μg/m^3, and 19.19–32.72%, respectively. The *CV-R*^{2} decreased, and *CV-RMSPE* and *CV-RPE* increased, indicating that the model had a slight overfitting. In addition, **Figure 4** shows that, when the measured [$PM_{2.5}$] exceeds 400 μg/m^3, the model had a slight "high value underestimation" phenomenon.

During the study period, the model performed best in 2020. Under the regression of the observed and predicted [$PM_{2.5}$] in the study area, *CV-R*^{2} was the highest at 0.95, and the *CV-RMSPE* and *CV-RPE* were the lowest at 7.87 μg/m^3 and 19.19%, respectively. This is mainly attributable to the government's series of "Air Pollution Prevention and Control Action Plans" (APPCAP), and the [$PM_{2.5}$] has been declining year by year. About 93.72% of [$PM_{2.5}$] data samples in 2020 were less than 100 μg/m^3. In contrast, the model performed the worst in 2013, with the lowest *CV-R*^{2} and the largest forecast uncertainty. The main reason was that more than 32.38% of the data samples were more than 100 μg/m^3, and relatively discrete data samples increased the difficulty of model fitting. Overall, the LME + GWR model that we have established was robust. Using the LME + GWR model combined with the 1-km MAIAC AOD product could excellently predict the daily near-surface [$PM_{2.5}$] with *CV-R*^{2} > 0.84, *CV-RMSPE* < 30 μg/m^3, and *CV-RPE* < 33% in the BTH.

Spatiotemporal Patterns of $PM_{2.5}$ Concentrations

Annual Variations

Figure 5 illustrated the annual mean [$PM_{2.5}$] estimated by the LME + GWR model, and ground-level observed [$PM_{2.5}$] from 2013 to 2020 in the BTH. The spatial variation pattern of [$PM_{2.5}$] estimated by the model was in good agreement with ground observations. The low-value areas of [$PM_{2.5}$] were located in the western and northern mountainous areas (Zone I), and the high-value areas were located in the middle and south of the BTH inland plain (Zone II). In general, the [$PM_{2.5}$] present a spatial distribution pattern of "low in the northern mountains and high in the southern plains". During the study period, the annual mean [$PM_{2.5}$] were 69.67, 65.31, 49.26, 51.17, 44.96, 43.11, 34.54, and 32.02 μg/m^3, respectively, and the overall $PM_{2.5}$ pollution level dropped significantly. Moreover, high-concentration areas ([$PM_{2.5}$] > 75 μg/m^3) have shrunk remarkably, and polluted cities were mainly concentrated in Handan, Xingtai, Shijiazhuang, and Baoding.

We adopted linear regression method to analyze the trends of annual mean [$PM_{2.5}$] in BTH. **Figure 6** illustrates the spatial distribution of the slope and significance level of [$PM_{2.5}$] from 2013 to 2020. Most of the mountain areas (Zone I) in the BTH failed the significance test ($p \geq 0.01$). The reason was speculated that the [$PM_{2.5}$] changed slightly during the study period. In addition, the [$PM_{2.5}$] level showed a significant decreasing trend ($p < 0.05$) in inland and coastal areas (Zone II and Zone III).

Seasonal Variations

$PM_{2.5}$ pollution in the BTH displayed strong seasonal variability. On the whole, the [$PM_{2.5}$] presented the seasonal variation characteristics of "high concentration in winter, low concentration in summer, and transition between spring and autumn" (**Figure 7**). During the study period in winter, the mean [$PM_{2.5}$] were 117.46, 84.24, 75.30, 72.72, 55.97, 52.75, 51.48, and 51.42 μg/m^3, respectively. There was a sharp decline in pollution from 2015 to 2017 and a steady decline after 2017. Compared with the [$PM_{2.5}$] in the winter of 2013, there was a decrease of 61 μg/m^3 (52%) in 2017 and 66 μg/m^3 (56%) in 2020. In addition, the annual and seasonal mean [$PM_{2.5}$] in the Zone II dropped the fastest compared with Zone I and Zone III (**Figure 8**).

Monthly Variations

During the study period, the estimated monthly [$PM_{2.5}$] of each year presented a U-shaped pattern (**Figure 9**), which was consistent with

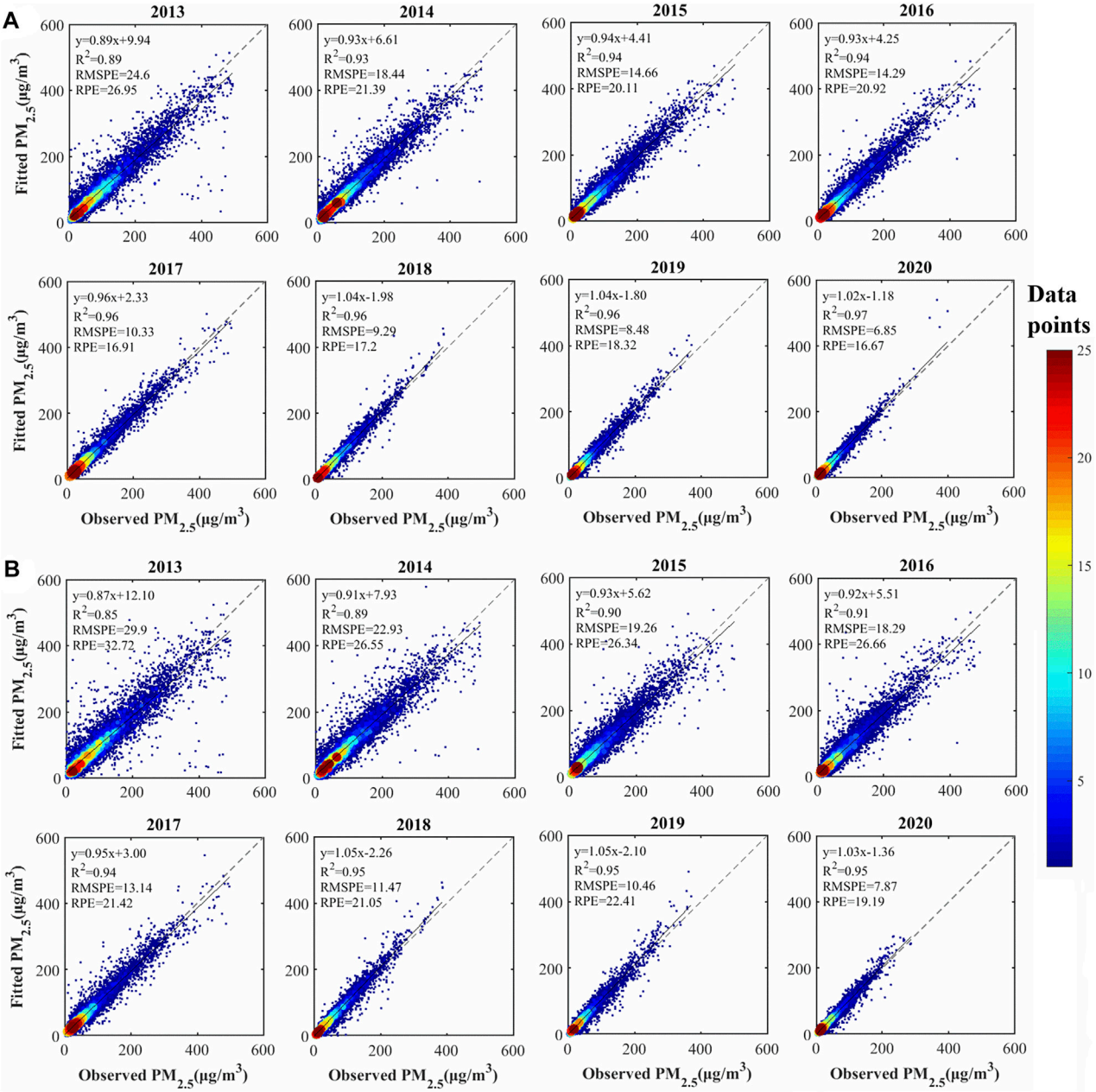

FIGURE 4 | Comparison of model fitting **(A)** and 10-fold cross-validation **(B)** results from 2013 to 2020.

the monthly measured [$PM_{2.5}$] distribution (**Figure 3**). January and December were the two months with the highest monthly mean [$PM_{2.5}$], which were related to coal-fired heating in the BTH. In addition, the low atmospheric humidity and temperature in these two months were also an important reason.

For the spatial distribution, the mean monthly [$PM_{2.5}$] had significant differences (**Figure 10**). The [$PM_{2.5}$] from May to September remained at a relatively low level. From October to February of the next year, cities in inland plain areas (e.g., Shijiazhuang, Baoding, Handan, and Xingtai) had the high-level [$PM_{2.5}$].

Figure 11 represents the daily fluctuations of [$PM_{2.5}$] based on station measurements and model estimates in Beijing and Shijiazhuang. The [$PM_{2.5}$] estimated by LME + GWR from 2013 to 2020 had excellent consistency with the monitoring station data and merely appeared a "high value underestimated" prediction deviation at few high concentrations (more than 400 μg/m^3). The fluctuation pattern of $PM_{2.5}$ pollution in Shijiazhuang was identical with Beijing. The peak values of [$PM_{2.5}$] were mainly distributed in winter, and the peak value in Shijiazhuang (the highest of 492.28 μg/m^3 appeared in 2014) was higher than that in Beijing (the highest of 463.52 μg/

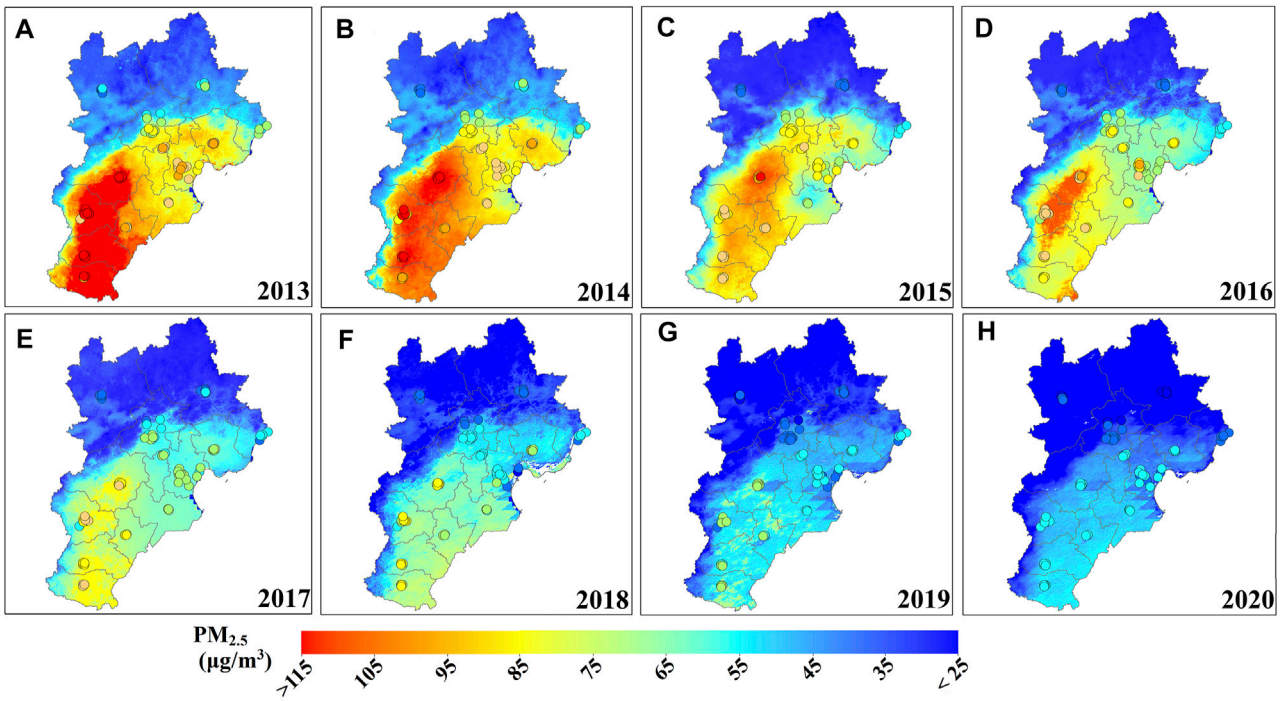

FIGURE 5 | The distribution of the annual mean estimated $PM_{2.5}$ concentrations and observed $PM_{2.5}$ concentrations in the Beijing–Tianjin–Hebei region during 2013–2020 **(A–H)**.

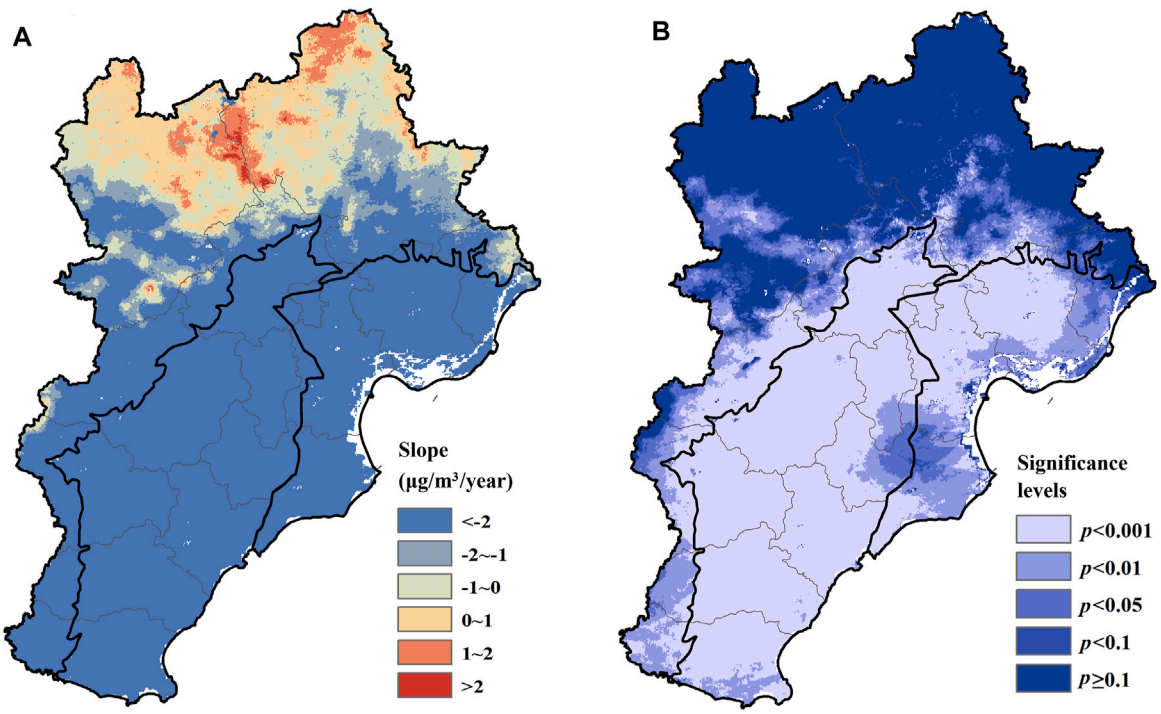

FIGURE 6 | Spatial distributions of the slope **(A)** and significance levels **(B)** of annual mean $PM_{2.5}$ concentrations in the Beijing–Tianjin–Hebei region from 2013 to 2020.

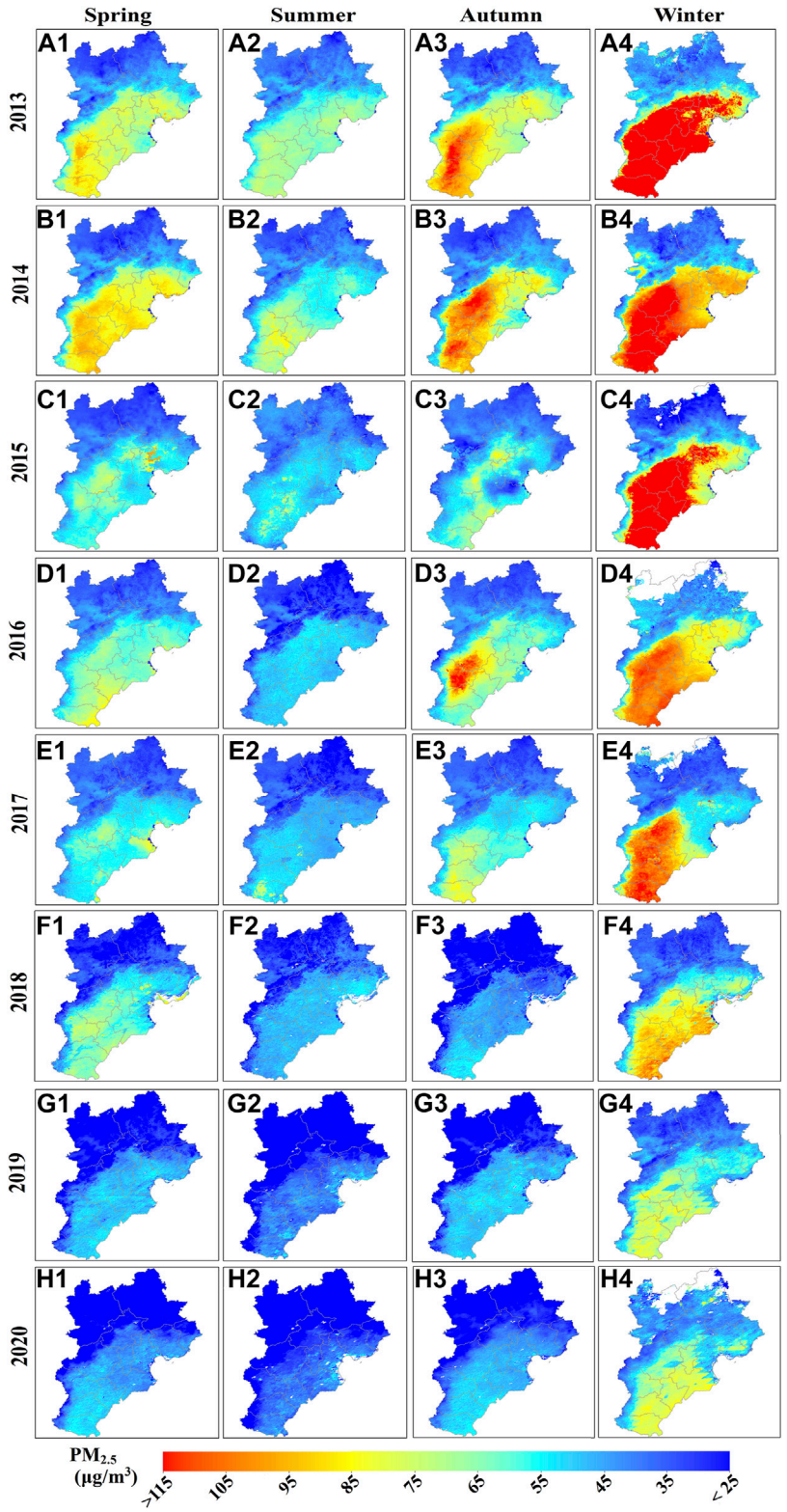

FIGURE 7 | Distribution of mean $PM_{2.5}$ concentrations in spring **(A1–H1)**, summer **(A2–H2)**, autumn **(A3–H3)**, and winter **(A4–H4)** in the Beijing–Tianjin–Hebei region during 2013–2020.

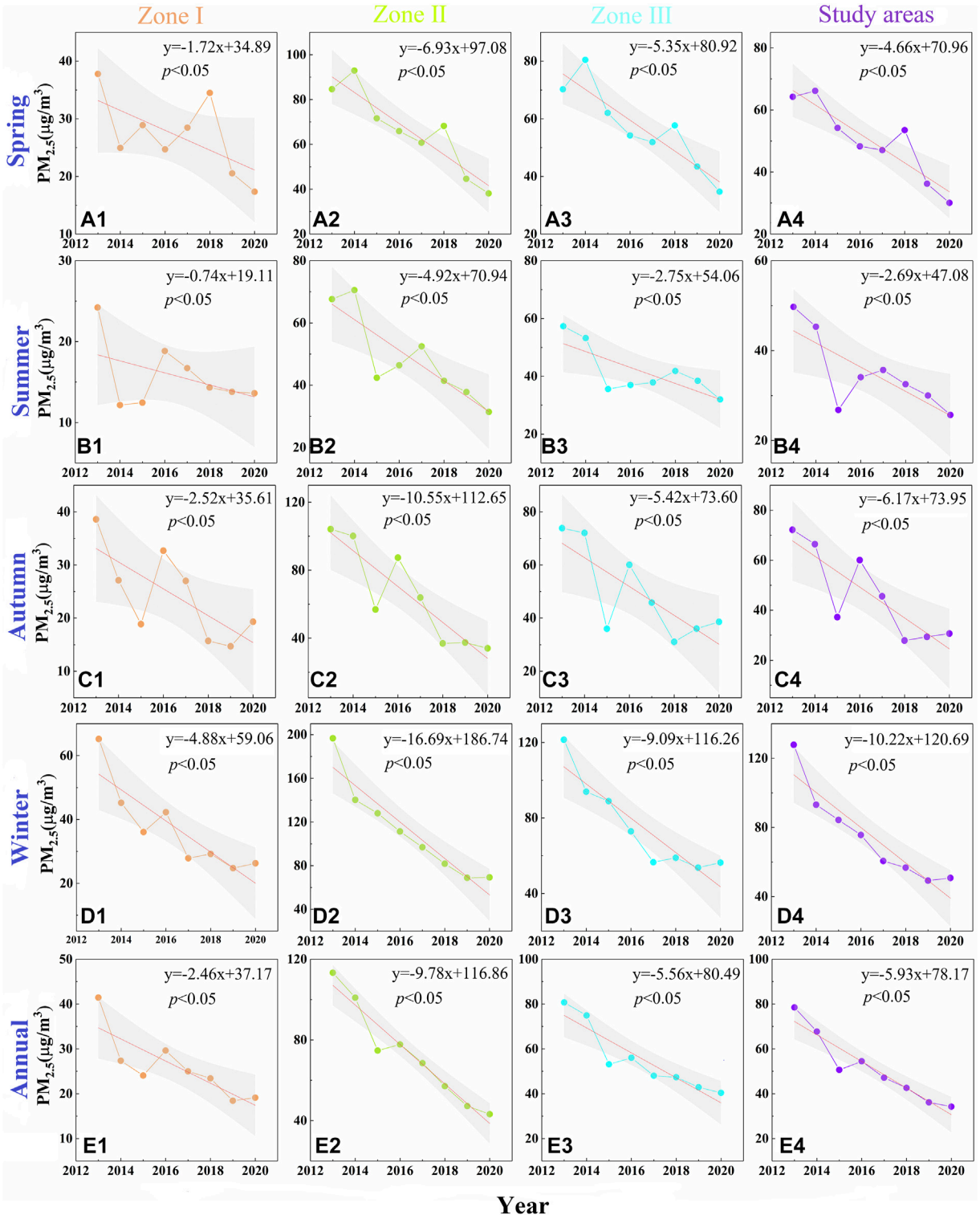

FIGURE 8 | Scatter plots of seasonal and annual trends of $PM_{2.5}$ concentrations in the Zone I **(A1–E1)**, Zone II **(A2–E2)**, Zone III **(A3–E3)**, and the Beijing–Tianjin–Hebei region **(A4–E4)** from 2013 to 2020. (The gray band represents the 95% confidence interval).

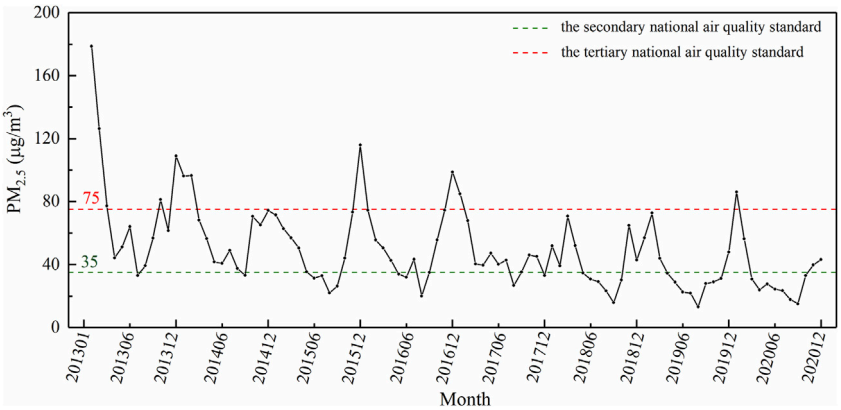

FIGURE 9 | Statistical variations of the monthly mean $PM_{2.5}$ concentrations in the Beijing–Tianjin–Hebei region from 2013 to 2020.

m^3 appeared in 2015). During the study period, the annual mean [$PM_{2.5}$] in Beijing were 57.54, 54.34, 54.30, 54.53, 54.38, 39.07, 30.87, and 30.09 μg/m^3, which were lower than 108.40, 91.61, 69.31, 74.48, 67.63, 53.63, 43.52, and 39.87 μg/m^3 in Shijiazhuang. However, $PM_{2.5}$ fell sharply in Shijiazhuang, with a drop of 63.21% from 2013 to 2020. In addition, the frequency of high pollution in Shijiazhuang in winter was higher than that in Beijing.

DISCUSSION

Causes Affecting the Spatiotemporal Distributions of $PM_{2.5}$

During the period from 2013 to 2020, [$PM_{2.5}$] in the BTH showed obvious spatiotemporal variations on different scales of annual, seasonal, and monthly. Overall [$PM_{2.5}$] in the BTH revealed a downward trend during the investigated period. Exploring the reasons for the decrease in the [$PM_{2.5}$] was inseparable from the national policy control, such as coal-to-gas and energy-saving transformation (Pan et al., 2021). In detail, the APPCAP implemented between 2013 and 2017 has successfully reduced [$PM_{2.5}$] (Yue et al., 2020), and the sharp decline in 2017 was closely related to the termination year of the APPCAP in 2017. Moreover, the [$PM_{2.5}$] in December 2015 and December 2016 were significantly higher than that in other years. The reason was that El Niño in 2015 enhanced the winter air pollution in northern China (Chang et al., 2016). The high concentration in the winter of 2016 might be influenced by anthropogenic factors (Ding et al., 2021). In addition, the [$PM_{2.5}$] in the winter of 2018–2020 decreased slowly compared with 2017, and the light-pollution areas (such as Langfang and Tangshan) slightly expanded. Furthermore, combined with the contribution of the suspension of work and production during new coronavirus disease (COVID-19) (Xian et al., 2021), the [$PM_{2.5}$] in the winter of 2020 dropped to 51.42 μg/m^3, which was the lowest [$PM_{2.5}$] in winter during the study period.

In the BTH, [$PM_{2.5}$] presented the significant seasonal variation characteristics of "high in winter, low in summer, and transition between spring and autumn", which were consistent with previous studies (Wu et al., 2016; Guo et al., 2021; Lu et al., 2021). The high [$PM_{2.5}$] in winter was concentrated in cities such as Shijiazhuang, Xingtai, and Handan. In the study areas, pollutant emissions were mainly due to the coal-fired heating and unfavorable meteorological conditions (Lv et al., 2017). Relevant studies have pointed out that the increase of boundary layer height and higher water vapor content in summer are the main reasons for the low [$PM_{2.5}$] (Qu et al., 2016; Ding et al., 2021). Moreover, the elevated [$PM_{2.5}$] levels in autumn were likely caused by the large scale straw burning in the rural areas and coal burning for heating in November (Duan et al., 2004; Lv et al., 2017). In addition, the spatiotemporal variation trends on the monthly scale follow the characteristics of seasonal changes, with the most polluted months appearing in December and January.

Comparisons With Other Studies in the Beijing–Tianjin–Hebei Region

In previous studies, the *CV-*R^2 value range of the satellite-based ground [$PM_{2.5}$] estimation model for the BTH was 0.54–0.95 (**Table 4**). Among these, the [$PM_{2.5}$] estimation model based on MODIS MAIAC AOD (*CV-*R^2 up to 0.82–0.95) has been found to perform better than other [$PM_{2.5}$] estimation models (a maximum *CV-*R^2 of 0.83), owing to its superior spatial resolution. Under the same high spatial resolution of AOD, our model showed similar or even better performance than other machine learning models. The performance statistics of the LME + GWR model developed was also comparable with other studies conducted in the United States that used the MODIS MAIAC AOD data (*CV-*R^2 up to 0.62–0.84) (Hu et al., 2014a, 2014b; Chudnovsky et al., 2014; Stowell et al., 2020). For model, the LME model cannot estimate the daily value of $PM_{2.5}$ at non-monitoring points, even if there are abundant data available. Models such as TEFR and STLME also have this shortcoming (Wu et al., 2016; Wang W. et al., 2021). In addition, machine learning methods that account for complex nonlinear relationships between different variables by adding hidden nodes and layers exhibited good performance in estimating [$PM_{2.5}$] (Ni et al., 2018; Stafoggia et al., 2019; Sun et al., 2019; Zhao et al., 2020; Ding et al., 2021). However, the

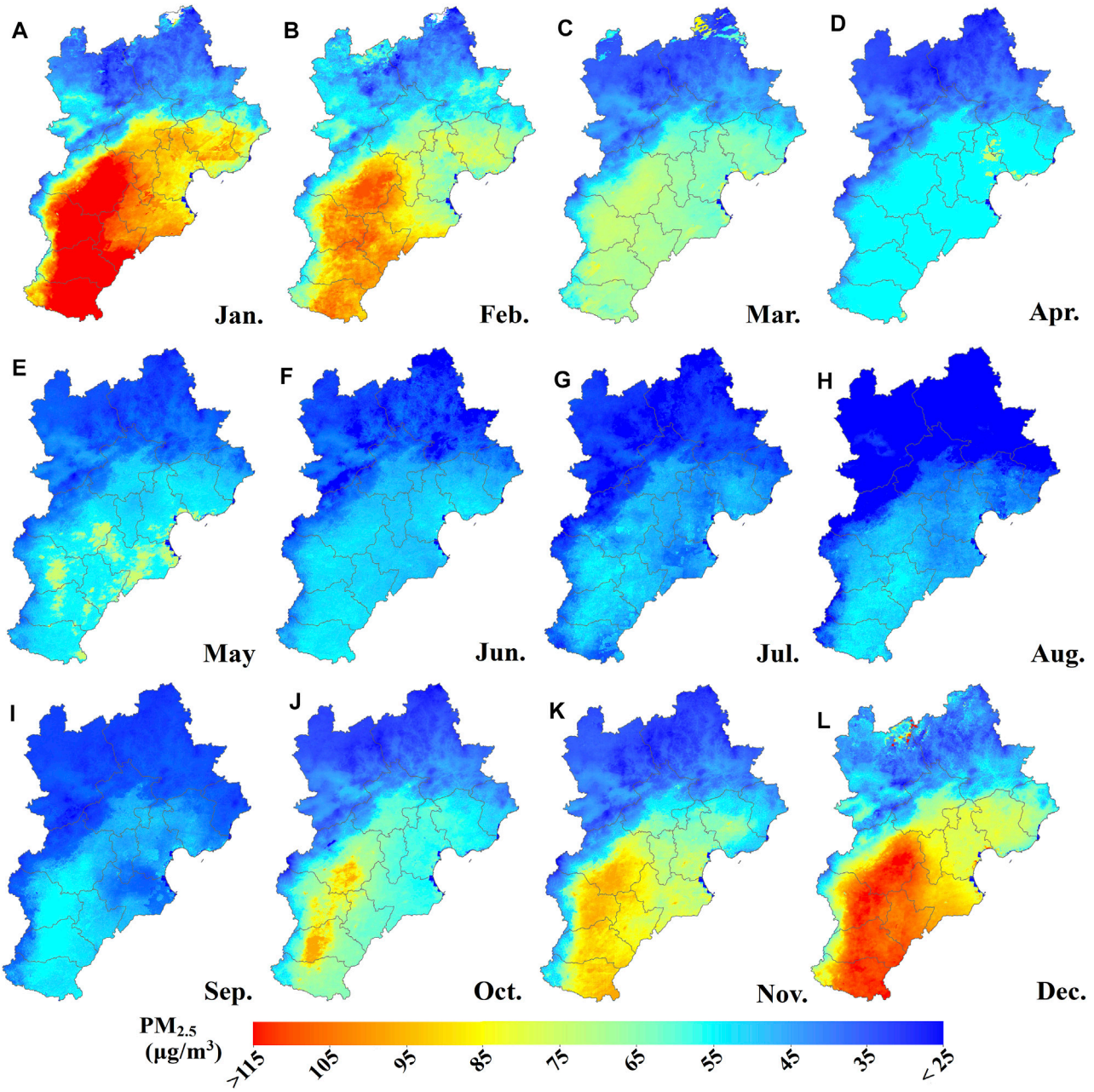

FIGURE 10 | Spatial distributions of monthly mean $PM_{2.5}$ concentrations **(A–L)** in the Beijing–Tianjin–Hebei region during 2013–2020.

addition of more hidden nodes and layers consumed a lot of time in estimating $PM_{2.5}$ load and produced different results for each training (Wang W. et al., 2021). Therefore, the LME + GWR model has certain advantages in terms of performance and stability. For AOD product, AHI AOD was commonly used to estimate hourly [$PM_{2.5}$] due to its high resolution. However, AHI cannot retrieve AOD at nighttime, and the quality is slightly inferior to MODIS AOD (Sun et al., 2019; Wang W. et al., 2021).

The model proposed in this study has many advantages. First, the high spatiotemporal resolution MAIAC Terra/Aqua fusion AOD data were employed in the model and achieved satisfactory performance. Second, the AOD quadratic term (AOD^2) and the interaction term of AOD and PBLH (PBLH×AOD) were introduced into the first-stage LME model to describe the nonlinear effect of the model. Third, we adopted the GWR model as the second-stage model to improve the spatial difference of the $PM_{2.5}$–AOD. The bisquare kernel bandwidth function and adaptive bandwidth method were selected owing to the difference between the daily sample data. After CV, the degree of overfitting was very small (compared with R^2, CV-R^2 was only reduced by 0.01–0.04).

However, the model still has some limitations. One limitation was the mismatch in spatial resolution between MODIS MAIAC AOD

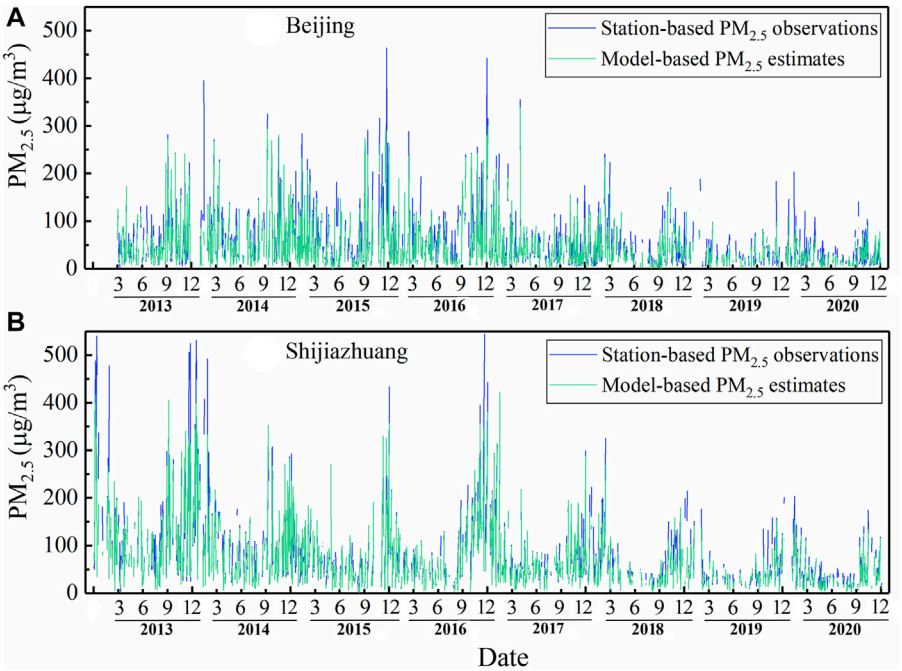

FIGURE 11 | Daily fluctuation in $PM_{2.5}$ concentrations based on station observations and model-based estimates in Beijing **(A)** and Shijiazhuang **(B)**.

TABLE 4 | Performances of previous studies on $PM_{2.5}$ estimates in the Beijing–Tianjin–Hebei region.

Related study	Spatial resolution (km)	Time period	Model	Model-fitting		Cross-validation		AOD source
				R^2	RMSPE	R^2	RMSPE	
Wang et al. (2019)	10	2017	LME	0.81	24.48	0.78	26.69	MODIS, NAQPMS
Wu et al. (2016)	6	2014	TEFR + GWR	0.88	13.05	0.71	19.29	VIIRS
Wang et al. (2021b)	5	2018	STLME	0.88	17.10	0.83	20.90	AHI
Ni et al. (2018)	3	2014–2016	BPNN	0.68	20.99	0.54	24.13	MODIS
He and Huang (2018b)	3	2013–2015	iGTWR	0.88	24.22	0.82	29.96	MODIS
Sun et al. (2019)	1	2017	DNN	0.91	14.27	0.84	19.90	AHI
Zhao et al. (2020)	1	2010-–2016	RF	0.86	23.48	0.83		MODIS
Ding et al. (2021)	1	2015–2019	CatBoost	-	-	0.88	17.79	MODIS
This study	1	2013–2020	LME + GWR	0.89–0.97	6.85–24.60	0.85–0.95	7.87–29.90	MODIS

BPNN, iGTWR, and DNN are the back propagation neural network model, improved geographically and temporally weighted regression model, and the deep neural networks model, respectively.

(0.01° × 0.01°) and meteorological parameters (0.1° × 0.1° and 0.0625° × 0.0625°). Although the bilinear interpolation method for meteorological factors has proved to have better performance than linear interpolation and nearest neighbor interpolation algorithms (Zhao et al., 2020), more meteorological products with high spatial resolution were still needed. Another limitation was that we only keep three data records in some days to bring into the model. Related studies have pointed out that the overfitting degree of the two-stage model incorporating GWR decreases with the increase in the number of matching data records per day (Hu et al., 2014a; Wu et al., 2016). Therefore, too few observations in some days would lead to the GWR model to overfitting. We will explore the optimal threshold that matches the minimum number of data records later. In addition, some studies have indicated that $PM_{2.5}$ monitoring stations mostly located in cities and suburbs, and the $PM_{2.5}$ estimation in mountainous and rural areas was relatively poor (Zeng et al., 2020; Ding et al., 2021). Our study area is in the BTH with characteristics of urban industrial conditions. In particular, Hebei Province that has many rural administrative units also has a large number of factories. Provincial monitoring sites with a larger coverage area should be added to future research to increase the regional representation of the sample.

CONCLUSION

In this study, the two-stage model (LME + GWR) that applied MODIS MAIAC AOD and measured [$PM_{2.5}$] and

meteorological and LU data as input variables was constructed to estimate the daily [$PM_{2.5}$] from 2013 to 2020 in the BTH. The LME + GWR model presented satisfactory performance ($CV\text{-}R^2$ was 0.85–0.95, *RMSPE* was 7.87–29.90 μg/m^3, and *RPE* was 19.19–32.71%) and provided a well-documented dataset for air pollution monitoring. During the investigated period from 2013 to 2020, $PM_{2.5}$ pollution in the BTH region has generally been on a downward trend. This decline is mainly due to anthropogenic factors such as pollution-preventing policies, but natural factors such as climate phenomenon (El Niño) also have a certain effect. In particular, in winter season, the [$PM_{2.5}$] exhibited relatively small fluctuations from 2013 to 2014, a sharp decline occurred from 2015 to 2017, and a steady decline from 2018 to 2020.

DATA AVAILABILITY STATEMENT

The original contributions presented in the study are included in the article/**Supplementary Material**, further inquiries can be directed to the corresponding authors.

AUTHOR CONTRIBUTIONS

DX and WW had the idea for the article and critically revised the work; XY performed the data processing and analysis; HB and JT gave many suggestions for this paper; XY, DX, and WW prepared the manuscript. All authors read and approved the final manuscript.

FUNDING

This work was supported by the National Natural Science Foundation of China (no.41471091) and the High-level Talents Training and Subsidy Project of Hebei Academy of Science (202201).

SUPPLEMENTARY MATERIAL

The Supplementary Material for this article can be found online at: https://www.frontiersin.org/articles/10.3389/fenvs.2022.842237/full#supplementary-material

REFERENCES

Bai, Y., Wu, L., Qin, K., Zhang, Y., Shen, Y., and Zhou, Y. (2016). A Geographically and Temporally Weighted Regression Model for Ground-Level PM2.5 Estimation from Satellite-Derived 500 M Resolution AOD. *Remote Sensing* 8 (3), 262. doi:10.3390/rs8030262

Chang, L., Xu, J., Tie, X., and Wu, J. (2016). Impact of the 2015 El Nino Event on Winter Air Quality in China. *Sci. Rep.* 6, 34275. doi:10.1038/srep34275

Chen, B., You, S., Ye, Y., Fu, Y., Ye, Z., Deng, J., et al. (2021). An Interpretable Self-Adaptive Deep Neural Network for Estimating Daily Spatially-Continuous PM2.5 Concentrations across China. *Sci. Total Environ.* 768, 144724. doi:10.1016/j.scitotenv.2020.144724

China, M. E. P. (2012). *Ambient Air Quality Standards. GB 3095-2012*. Beijing: China Environmental Science Press.

Choi, M., Lim, H., Kim, J., Lee, S., Eck, T. F., Holben, B. N., et al. (2019). Validation, Comparison, and Integration of GOCI, AHI, MODIS, MISR, and VIIRS Aerosol Optical Depth over East Asia during the 2016 KORUS-AQ Campaign. *Atmos. Meas. Tech.* 12 (8), 4619–4641. doi:10.5194/amt-12-4619-2019

Chow, J. C., Watson, J. G., Mauderly, J. L., Costa, D. L., Wyzga, R. E., Vedal, S., et al. (20062006). Health Effects of Fine Particulate Air Pollution: Lines that Connect. *J. Air Waste Manage. Assoc.* 56 (10), 1368–1380. doi:10.1080/10473289.2006.10464545

Chudnovsky, A. A., Koutrakis, P., Kloog, I., Melly, S., Nordio, F., Lyapustin, A., et al. (2014). Fine Particulate Matter Predictions Using High Resolution Aerosol Optical Depth (AOD) Retrievals. *Atmos. Environ.* 89, 189–198. doi:10.1016/j.atmosenv.2014.02.019

Ding, Y., Chen, Z., Lu, W., and Wang, X. (2021). A CatBoost Approach with Wavelet Decomposition to Improve Satellite-Derived High-Resolution PM2.5 Estimates in Beijing-Tianjin-Hebei. *Atmos. Environ.* 249, 118212. doi:10.1016/j.atmosenv.2021.118212

Duan, F., Liu, X., Yu, T., and Cachier, H. (2004). Identification and Estimate of Biomass Burning Contribution to the Urban Aerosol Organic Carbon Concentrations in Beijing. *Atmos. Environ.* 38, 1275–1282. doi:10.1016/j.atmosenv.2003.11.037

Engel-cox, J. A., Holloman, C. H., Coutant, B. W., and Hoff, R. M. (2004). Qualitative and Quantitative Evaluation of MODIS Satellite Sensor Data for Regional and Urban Scale Air Quality. *Atmos. Environ.* 38 (16), 2495–2509. doi:10.1016/j.atmosenv.2004.01.039

Engel-Cox, J., Kim Oanh, N. T., van Donkelaar, A., Martin, R. V., and Zell, E. (2013). Toward the Next Generation of Air Quality Monitoring: Particulate Matter. *Atmos. Environ.* 80, 584–590. doi:10.1016/j.atmosenv.2013.08.016

Gu, Y., Wong, T. W., Law, C. K., Dong, G. H., Ho, K. F., Yang, Y., et al. (2018). Impacts of Sectoral Emissions in China and the Implications: Air Quality, Public Health, Crop Production, and Economic Costs. *Environ. Res. Lett.* 13 (8), 084008. doi:10.1088/1748-9326/aad138

Guo, W., Zhang, B., Wei, Q., Guo, Y., Yin, X., Li, F., et al. (2021). Estimating Ground-Level PM2.5 Concentrations Using Two-Stage Model in Beijing-Tianjin-Hebei, China. *Atmos. Pollut. Res.* 12 (9), 101154. doi:10.1016/j.apr.2021.101154

Gupta, P., and Christopher, S. A. (2009). Particulate Matter Air Quality Assessment Using Integrated Surface, Satellite, and Meteorological Products: Multiple Regression Approach. *J. Geophys. Res.* 114, D14205. doi:10.1029/2008JD011496

He, Q., Gu, Y., and Zhang, M. (2020). Spatiotemporal Trends of PM2.5 Concentrations in central China from 2003 to 2018 Based on MAIAC-Derived High-Resolution Data. *Environ. Int.* 137, 105536. doi:10.1016/j.envint.2020.105536

He, Q., and Huang, B. (2018b). Satellite-based High-Resolution PM2.5 Estimation over the Beijing-Tianjin-Hebei Region of China Using an Improved Geographically and Temporally Weighted Regression Model. *Environ. Pollut.* 236, 1027–1037. doi:10.1016/j.envpol.2018.01.053

He, Q., and Huang, B. (2018a). Satellite-based Mapping of Daily High-Resolution Ground PM2.5 in China via Space-Time Regression Modeling. *Remote Sensing Environ.* 206, 72–83. doi:10.1016/j.rse.2017.12.018

Hu, X., Belle, J. H., Meng, X., Wildani, A., Waller, L. A., Strickland, M. J., et al. (2017). Estimating PM2.5 Concentrations in the Conterminous United States Using the Random Forest Approach. *Environ. Sci. Technol.* 51 (12), 6936–6944. doi:10.1021/acs.est.7b01210

Hu, X., Waller, L. A., Al-Hamdan, M. Z., Crosson, W. L., Estes, M. G., Jr, Estes, S. M., et al. (2013). Estimating Ground-Level PM2.5 Concentrations in the southeastern U.S. Using Geographically Weighted Regression. *Environ. Res.* 121, 1–10. doi:10.1016/j.envres.2012.11.003

Hu, X., Waller, L. A., Lyapustin, A., Wang, Y., Al-Hamdan, M. Z., Crosson, W. L., et al. (2014a). Estimating Ground-Level PM2.5 Concentrations in the Southeastern United States Using MAIAC AOD Retrievals and a Two-Stage Model. *Remote Sensing Environ.* 140, 220–232. doi:10.1016/j.rse.2013.08.032

Hu, X., Waller, L. A., Lyapustin, A., Wang, Y., and Liu, Y. (2014b). 10-year Spatial and Temporal Trends of PM2.5 Concentrations in the southeastern US Estimated Using High-Resolution Satellite Data. *Atmos. Chem. Phys.* 14 (12), 6301–6314. doi:10.5194/acp-14-6301-2014

Kahn, R., Banerjee, P., Mcdonald, D., and Diner, D. J. (1998). Sensitivity of Multiangle Imaging to Aerosol Optical Depth and to Pure-Particle Size Distribution and Composition over Ocean. *J. Geophys. Res.* 103 (D24), 32195–32213. doi:10.1029/98JD01752

Lee, H. J., Liu, Y., Coull, B. A., Schwartz, J., and Koutrakis, P. (2011). A Novel Calibration Approach of MODIS AOD Data to Predict PM2.5 Concentrations. *Atmos. Chem. Phys.* 11 (15), 7991–8002. doi:10.5194/acp-11-7991-2011

Li, T., Shen, H., Zeng, C., Yuan, Q., and Zhang, L. (2017). Point-surface Fusion of Station Measurements and Satellite Observations for Mapping PM2.5 Distribution in China: Methods and Assessment. *Atmos. Environ.* 152, 477–489. doi:10.1016/j.atmosenv.2017.01.004

Liang, F., Xiao, Q., Wang, Y., Lyapustin, A., Li, G., Gu, D., et al. (2018). MAIAC-based Long-Term Spatiotemporal Trends of PM2.5 in Beijing, China. *Sci. Total Environ.* 616-617, 1589–1598. doi:10.1016/j.scitotenv.2017.10.155

Liu, Y., Paciorek, C. J., and Koutrakis, P. (2009). Estimating Regional Spatial and Temporal Variability of PM 2.5 Concentrations Using Satellite Data, Meteorology, and Land Use Information. *Environ. Health Perspect.* 117 (6), 886–892. doi:10.1289/ehp.0800123

Liu, Y., Park, R. J., Jacob, D. J., Li, Q., Kilaru, V., and Sarnat, J. A. (2004). Mapping Annual Mean Ground-Level PM2.5concentrations Using Multiangle Imaging Spectroradiometer Aerosol Optical Thickness over the Contiguous United States. *J. Geophys. Res.* 109, a–n. doi:10.1029/2004jd005025

Lu, J., Zhang, Y., Chen, M., Wang, L., Zhao, S., Pu, X., et al. (2021). Estimation of Monthly 1 Km Resolution PM2.5 Concentrations Using a Random forest Model over "2 + 26" Cities, China. *Urban Clim.* 35, 100734. doi:10.1016/j.uclim.2020.100734

Lv, B., Hu, Y., Chang, H. H., Russell, A. G., Cai, J., Xu, B., et al. (2017). Daily Estimation of Ground-Level PM2.5 Concentrations at 4 Km Resolution over Beijing-Tianjin-Hebei by Fusing MODIS AOD and Ground Observations. *Sci. Total Environ.* 580, 235–244. doi:10.1016/j.scitotenv.2016.12.049

Lyapustin, A., Wang, Y., Korkin, S., and Huang, D. (2018). MODIS Collection 6 MAIAC Algorithm. *Atmos. Meas. Tech.* 11 (10), 5741–5765. doi:10.5194/amt-11-5741-2018

Ma, Z., Hu, X., Sayer, A. M., Levy, R., Zhang, Q., Xue, Y., et al. (2016). Satellite-Based Spatiotemporal Trends in PM 2.5 Concentrations: China, 2004-2013. *Environ. Health Perspect.* 124 (2), 184–192. doi:10.1289/ehp.1409481

Moazami, S., Noori, R., Amiri, B. J., Yeganeh, B., Partani, S., and Safavi, S. (2016). Reliable Prediction of Carbon Monoxide Using Developed Support Vector Machine. *Atmos. Pollut. Res.* 7 (3), 412–418. doi:10.1016/j.apr.2015.10.022

Ni, X., Cao, C., Zhou, Y., Cui, X., and P. Singh, R. (2018). Spatio-Temporal Pattern Estimation of PM2.5 in Beijing-Tianjin-Hebei Region Based on MODIS AOD and Meteorological Data Using the Back Propagation Neural Network. *Atmosphere* 9, 105. doi:10.3390/atmos9030105

Pan, X., Zhao, Y., and Wang, M. (2021). Impact of COVID-19 on Extremely Polluted Air Quality and Trend Forecast in Seven Provinces and Three Cities of China. *Front. Environ. Sci.* 9, 770900. doi:10.3389/fenvs.2021.770900

Polezer, G., Tadano, Y. S., Siqueira, H. V., Godoi, A. F. L., Yamamoto, C. I., de André, P. A., et al. (2018). Assessing the Impact of PM2.5 on Respiratory Disease Using Artificial Neural Networks. *Environ. Pollut.* 235, 394–403. doi:10.1016/j.envpol.2017.12.111

Qu, W., Wang, J., Zhang, X., Sheng, L., and Wang, W. (2016). Opposite Seasonality of the Aerosol Optical Depth and the Surface Particulate Matter Concentration over the North China Plain. *Atmos. Environ.* 127, 90–99. doi:10.1016/j.atmosenv.2015.11.061

Riediker, M., Franc, Y., Bochud, M., Meier, R., and Rousson, V. (2018). Exposure to Fine Particulate Matter Leads to Rapid Heart Rate Variability Changes. *Front. Environ. Sci.* 6, 2. doi:10.3389/fenvs.2018.00002

Schaap, M., Apituley, A., Timmermans, R. M. A., Koelemeijer, R. B. A., and de Leeuw, G. (2009). Exploring the Relation between Aerosol Optical Depth and PM2.5 at Cabauw, the Netherlands. *Atmos. Chem. Phys.* 9, 909–925. doi:10.5194/acp-9-909-2009

Stafoggia, M., Bellander, T., Bucci, S., Davoli, M., de Hoogh, K., de' Donato, F., et al. (2019). Estimation of Daily PM10 and PM2.5 Concentrations in Italy, 2013-2015, Using a Spatiotemporal Land-Use Random-forest Model. *Environ. Int.* 124, 170–179. doi:10.1016/j.envint.2019.01.016

Stowell, J. D., Bi, J., Al-Hamdan, M. Z., Lee, H. J., Lee, S.-M., Freedman, F., et al. (2020). Estimating PM2.5 in Southern California Using Satellite Data: Factors that Affect Model Performance. *Environ. Res. Lett.* 15 (9), 094004. doi:10.1088/1748-9326/ab9334

Sun, Y., Zeng, Q., Geng, B., Lin, X., Sude, B., and Chen, L. (2019). Deep Learning Architecture for Estimating Hourly Ground-Level PM2.5 Using Satellite Remote Sensing. *IEEE Geosci. Remote Sensing Lett.* 16 (9), 1343–1347. doi:10.1109/lgrs.2019.2900270

van Donkelaar, A., Martin, R. V., and Park, R. J. (2006). Estimating Ground-Level PM2.5using Aerosol Optical Depth Determined from Satellite Remote Sensing. *J. Geophys. Res.* 111, D21201. doi:10.1029/2005JD006996

Wang, G., Leng, W., Jiang, S., and Cao, B. (2021a). Long-Term Variation in Wintertime Atmospheric Diffusion Conditions over the Sichuan Basin. *Front. Environ. Sci.* 9, 763504. doi:10.3389/fenvs.2021.763504

Wang, J., and Christopher, S. A. (2003). Intercomparison between Satellite-Derived Aerosol Optical Thickness and PM2.5mass: Implications for Air Quality Studies. *Geophys. Res. Lett.* 30 (21), 2095. doi:10.1029/2003gl018174

Wang, Q., Zeng, Q., Tao, J., Sun, L., Zhang, L., Gu, T., et al. (2019). Estimating PM2.5 Concentrations Based on MODIS AOD and NAQPMS Data over Beijing-Tianjin-Hebei. *Sensors* 19 (5), 1207. doi:10.3390/s19051207

Wang, W., He, J., Miao, Z., and Du, L. (2021b). Space-Time Linear Mixed-Effects (STLME) Model for Mapping Hourly fine Particulate Loadings in the Beijing-Tianjin-Hebei Region, China. *J. Clean. Prod.* 292, 125993. doi:10.1016/j.jclepro.2021.125993

Wang, X., Sun, W., Zheng, K., Ren, X., and Han, P. (2020). Estimating Hourly PM2.5 Concentrations Using MODIS 3 Km AOD and an Improved Spatiotemporal Model over Beijing-Tianjin-Hebei, China. *Atmos. Environ.* 222, 117089. doi:10.1016/j.atmosenv.2019.117089

Wu, J., Yao, F., Li, W., and Si, M. (2016). VIIRS-based Remote Sensing Estimation of Ground-Level PM2.5 Concentrations in Beijing-Tianjin-Hebei: A Spatiotemporal Statistical Model. *Remote Sensing Environ.* 184, 316–328. doi:10.1016/j.rse.2016.07.015

Xian, T., Li, Z., and Wei, J. (2021). Changes in Air Pollution Following the COVID-19 Epidemic in Northern China: The Role of Meteorology. *Front. Environ. Sci.* 9, 654651. doi:10.3389/fenvs.2021.654651

Xiao, Q., Wang, Y., Chang, H. H., Meng, X., Geng, G., Lyapustin, A., et al. (2017). Full-coverage High-Resolution Daily PM2.5 Estimation Using MAIAC AOD in the Yangtze River Delta of China. *Remote Sensing Environ.* 199, 437–446. doi:10.1016/j.rse.2017.07.023

Xue, W., Zhang, J., Zhong, C., Ji, D., and Huang, W. (2020). Satellite-derived Spatiotemporal PM2.5 Concentrations and Variations from 2006 to 2017 in China. *Sci. Total Environ.* 712, 134577. doi:10.1016/j.scitotenv.2019.134577

Yan, J.-W., Tao, F., Zhang, S.-Q., Lin, S., and Zhou, T. (2021). Spatiotemporal Distribution Characteristics and Driving Forces of PM2.5 in Three Urban Agglomerations of the Yangtze River Economic Belt. *Ijerph* 18, 2222. doi:10.3390/ijerph18052222

Yang, K., and He, J. (2019). *China Meteorological Forcing Dataset (1979-2018)*. National Tibetan Plateau Data Center. doi:10.11888/AtmosphericPhysics.tpe.249369.file

Yang, W., He, Z., Huang, H., and Huang, J. (2021). A Clustering Framework to Reveal the Structural Effect Mechanisms of Natural and Social Factors on PM2.5 Concentrations in China. *Sustainability* 13 (3), 1428. doi:10.3390/su13031428

Yao, F., Si, M., Li, W., and Wu, J. (2018). A Multidimensional Comparison between MODIS and VIIRS AOD in Estimating Ground-Level PM2.5 Concentrations over a Heavily Polluted Region in China. *Sci. Total Environ.* 618, 819–828. doi:10.1016/j.scitotenv.2017.08.209

Yao, F., Wu, J., Li, W., and Peng, J. (2019). A Spatially Structured Adaptive Two-Stage Model for Retrieving Ground-Level PM2.5 Concentrations from VIIRS AOD in China. *ISPRS J. Photogrammetry Remote Sensing* 151, 263–276. doi:10.1016/j.isprsjprs.2019.03.011

Yeganeh, B., Hewson, M. G., Clifford, S., Knibbs, L. D., and Morawska, L. (2017). A Satellite-Based Model for Estimating PM2.5 Concentration in a Sparsely Populated Environment Using Soft Computing Techniques. *Environ. Model. Softw.* 88, 84–92. doi:10.1016/j.envsoft.2016.11.017

Yue, H., He, C., Huang, Q., Yin, D., and Bryan, B. A. (2020). Stronger Policy Required to Substantially Reduce Deaths from PM2.5 Pollution in China. *Nat. Commun.* 11, 1462. doi:10.1038/s41467-020-15319-4

Zeng, Q., Tao, J., Chen, L., Zhu, H., Zhu, S., and Wang, Y. (2020). Estimating Ground-Level Particulate Matter in Five Regions of China Using Aerosol Optical Depth. *Remote Sensing* 12, 881. doi:10.3390/rs12050881

Zhang, K., de Leeuw, G., Yang, Z., Chen, X., Su, X., and Jiao, J. (2019b). Estimating Spatio-Temporal Variations of PM2.5 Concentrations Using VIIRS-Derived AOD in the Guanzhong Basin, China. *Remote Sensing* 11 (22), 2679. doi:10.3390/rs11222679

Zhang, R., Di, B., Luo, Y., Deng, X., Grieneisen, M. L., Wang, Z., et al. (2018). A Nonparametric Approach to Filling Gaps in Satellite-Retrieved Aerosol Optical Depth for Estimating Ambient PM2.5 Levels. *Environ. Pollut.* 243 (Pt B), 998–1007. doi:10.1016/j.envpol.2018.09.052

Zhang, Z., Wu, W., Fan, M., Wei, J., Tan, Y., and Wang, Q. (2019a). Evaluation of MAIAC Aerosol Retrievals over China. *Atmos. Environ.* 202, 8–16. doi:10.1016/j.atmosenv.2019.01.013

Zhao, B., Wang, S., Ding, D., Wu, W., Chang, X., Wang, J., et al. (2019). Nonlinear Relationships between Air Pollutant Emissions and PM2.5-related Health Impacts in the Beijing-Tianjin-Hebei Region. *Sci. Total Environ.* 661, 375–385. doi:10.1016/j.scitotenv.2019.01.169

Zhao, C., Wang, Q., Ban, J., Liu, Z., Zhang, Y., Ma, R., et al. (2020). Estimating the Daily PM2.5 Concentration in the Beijing-Tianjin-Hebei Region Using a Random forest Model with a 0.01° × 0.01° Spatial Resolution. *Environ. Int.* 134, 105297. doi:10.1016/j.envint.2019.105297

Conflict of Interest: The authors declare that the research was conducted in the absence of any commercial or financial relationships that could be construed as a potential conflict of interest.

Publisher's Note: All claims expressed in this article are solely those of the authors and do not necessarily represent those of their affiliated organizations or those of the publisher, the editors, and the reviewers. Any product that may be evaluated in this article, or claim that may be made by its manufacturer, is not guaranteed or endorsed by the publisher.